Egyptian Journal of Soil Science

http://ejss.journals.ekb.eg/

Effect of calcium silicate nanoparticles applications on salt affected soils environmental conditions

Doaa T. Eissa
Soil Physics and Chemistry dept., Water resources and desert land division, Desert Research Center, Cairo, P.O.B 11753, Egypt

$\mathbf{I}$N THE PRESENT study, various calcium silicate nanoparticles (NPs) were examined to decrease the impact of salinity on the grown plants by adsorbing Na^+ and borate (BO_3^{-3}) from water and soil. The Ca silicate was prepared using a green synthesis technique and subsequently activated by different acids, such as HNO_3 and H_3PO_4, producing Ca silicate-NO_3 NPs and Ca silicate-PO_4 NPs, respectively. The characterization of the prepared samples was conducted by X-ray powder diffraction (XRD), scanning electron microscopy (SEM), Fourier-transform infrared spectroscopy (FTIR), and dynamic light scattering (DLS). The removal of Na^+ and BO_3^{-3} from solutions was examined by activated calcium silicate NPs, considering different factors such as Na^+ and BO_3^{-3} concentrations, adsorption time, solution pH, and temperature. The results highlighted that the maximum removal of Na^+ (18.78%) was achieved by using Ca silicate NPs at an equilibrium contact time of 6 h, a concentration of 20 ppm, a pH of 8.1, and a temperature of 298 K. For BO_3^{-3}, the maximum removal of (22.47%) was observed at an equilibrium contact time of 6 hours, a concentration of 54.54 ppm, a pH of 6.08, and a temperature of 308.5 K. Freundlich and Langmuir isotherm models were utilized to analyze the experimental data. According to the findings, the Langmuir isotherm model more accurately characterized the experimental data. The adsorption kinetics were studied using the pseudo-first-order and pseudo-second-order models, revealing that the pseudo-second-order model best explained the adsorption kinetics. Furthermore, the study assessed the application of three levels (0, 4, and 8 g pot^{-1}) of Ca silicate NPs, Ca silicate-NO_3 NPs, and Ca silicate-PO_4 NPs to the dill plants (*Anethum graveolens* L.). Evaluation parameters include fresh and dry weight, Na, B, Ca, and Si concentrations, and plant tissue trace elements. A significant effect was observed between the concentrations of Na^+ in the plant and calcium silicate NPs additives. Regarding boron, adding calcium silicate reduced plants' absorbed amounts.

Keywords: Calcium silicate NPs ; Salt affected soil; Dill plant (*Anethum graveolens L.*); Adsorption.

1. Introduction

Salinity and sodicity impact 10% of the overall arable land, whereas 25–30% of irrigated lands are considered salt-affected and commercially unproductive. Reports indicated that 20% of the world's arable land and 50% of its farmland are damaged by salts (Zaman *et al*., 2018; Kumar, 2012). A portion of irrigated land is lost each year due to salinization issues. More than 800 million hectares, representing over 6% of all land, suffer from either salinity or sodicity, according to the Food and Agriculture Organization's (FAO) Land and Nutrition Management Service (2008). In Africa, the amount of salt-affected soil is 38.7 million hectares (2% of the total area). Meanwhile, 8.70 million hectares in Egypt, representing 8.7% of the total area, are affected by salt-related issues, as per FAO (FAO, 2003).

Salt-affected soils, divided into three categories: saline, saline-sodic, and sodic soils, represent a critical natural resource for expanding Egypt's agricultural land. Saline soils are characterized by an electrical conductivity of more than 4 dS.m^{-1} in saturation extract, an exchangeable sodium percentage (ESP) of less than 15, and a pH often lower than 8.5. Saline-sodic soils exhibit EC$_e$ higher than 4 dS.m^{-1}, ESP exceeding 15, and a pH rarely above 8.5. Meanwhile, the sodic/alkaline soils are identified by ESP values greater than 15, EC$_e$ less than 4 dS.m^{-1}, and a pH typically between 8.5 and 10 (Richard, 1954).

High salinity can alter the mineral nutrition of plants, leading to ion toxicity. Stress is significantly exacerbated by high salt content in the soil and water, especially in arid regions (Awad *et al.*, 2022; Abdrabou *et al.*, 2022). Egypt, experiencing the Mediterranean environment with frequent temperature changes, has been separated into several agro-climatic zones based on the average temperature values (Swelam *et al.*, 2022; Jalhoum *et al.*, 2022).

Water availability is a crucial environmental component for crop plant productivity, and water

scarcity is predicted to negatively impact the use of 25% of the world's land for agriculture (Delfine *et al.*, 2005; El-Sherpiny *et al.*, 2023). Abiotic stressors, such as drought and salinity, negatively influence plant fitness and performance, amplified by climatic change and environmental extremes (Singh *et al.*, 2018). Salinity and boron toxicity frequently coincide and interact with the responses of plants, as saline groundwater with high boron contents is used for irrigation worldwide (Grattan *et al.*, 2015). Crop productivity is impacted by agricultural issues such as boron poisoning (Bonilla and González-Fontes, 2011).

Rice is the leading food consumed by over half of the world's population and represents the primary dietary energy source for eight countries in Africa, 17 countries in Asia and the Pacific, and nine countries in North and South America (Shelke *et al.,* 2010). Rice contributes to 20% of the dietary energy consumed worldwide. However, if not appropriately used, rice straw, which constitutes roughly 3.5 million tons of the country's annual agricultural waste, might cause environmental problems. Among the most agro-wastes, rice husk ash is one of the most silica-rich raw materials, holding between 90 and 98% of silica after complete burning. According to Todkar *et al.* (2016), the ash produced from rice husks causes environmental problems.

Although silicon is the second most common element in the earth's crust, it is not thought to be a necessary component for plants, particularly when they face environmental and abiotic challenges such as drought and salinity (Debona *et al.*, 2017; Abd-Elzaher *et al.,* 2022).

The dill plant (*Anethum graveolens* L.), with a rich history of usage in traditional medicine, is frequently grown in dry and semi-arid areas with salt problems (Sukhdev *et al.*, 2006). It is a significant member of the Apeaceae family and is native to the Mediterranean and West Asia. This plant is grown for its edible fruits and vegetables as well as for its essential oil. According to Simon *et al.* (1984), it offers medical benefits as an antispasmodic, carminative, diuretic stimulant, and stomachic.

The present work aims to investigate the effects of calcium silicate NPs as soil ameliorants to mitigate the effects of salt-affected soils and improve agricultural productivity. Furthermore, our study aimed to manage agricultural waste, such as rice husk, to reduce its potential risks with the possibility of recycling. Finally, the study examined the best methods for removing Na^+ and BO_3^{-3} from solution using calcium silicate NPs.

2. Material and Methods
2.1. Soil sampling and analysis
In Burg El-Arab, Egypt, at 30° 44' 21.48" N and 29° 37' 24.60" E, the soil samples under consideration were collected from the surface layer (0–30 cm). The soil was air-dried, crushed, and then sieved using a 2-mm sieve. The soil texture was determined using the

international pipette method. According to the Walkley and Black method, the total organic matter content was calculated (%). The soil's pH and EC were measured in the soil paste. Total carbonate content (%) was volumetrically determined by Collin's calcimeter method (Jachson, 1973). The available elements in the soil sample were implemented following the procedure conducted by Gavlak *et al.* (2005). After digestion, the total elements content was detected using an inductively coupled plasma emission spectrophotometer (ICPseq-7500). The following equation (1) was used to estimate the sodium adsorption ratio (SAR) (USDA, 2014):

$$SAR = \frac{Na}{\sqrt[2]{\frac{Ca+Mg}{2}}} \qquad (1)$$

Where the concentrations of measured elements are in meq L-1 at saturation extracts.

Furthermore, the following equation (2) was used to calculate the ESP:

$$ESP = \frac{100(-0.0126 + 0.01475SAR)}{1 + (-0.0126 + 0.01475SAR)} \qquad (2)$$

2.2. Preparation of calcium silicate NPs
The silicon solution was prepared by washing the rice husk in distilled water, drying it at 60 ℃, crushing it into a fine powder, and then burning it for eight hours at 900 ℃ to produce rice husk ash. Then, 5.5 g of the rice husk ash was transferred into a 0.5 L stoppered flask containing an 18% KOH solution. The mixture was kept at 120°C for 2 hours before filtering through filter paper.

The calcium chloride (0.3 M) was dissolved in distilled water to create a calcium chloride solution. The silica solution obtained from filtration was mixed with the calcium chloride solution to create calcium silicate NPs. The mixed solution was stirred continuously and dried at 120 °C for 24 hours. The product was centrifuged, cleaned with deionized water multiple times, and adjusted to a consistent pH of 7 before dehydrating in an air oven for 24 hours at 80 °C, reaching a stable weight. The product was heated for three hours at 600 °C to eliminate any remaining organic molecules. Nitric and phosphoric acids were used to add functional groups to the surface or structure of the synthetic calcium silicate NPs, facilitating binding elements. This stage included treating the initial form of the product (Ca silicate NPs) with an excess volume of 0.1M HNO_3 and 0.1M H_3PO_4 solution at 60 °C using a water bath. Two different treated forms of calcium silicate were prepared: Ca silicate-NO_3 NPs and Ca silicate-PO_4 NPs. All NPs products underwent filtering, distilled water washing, air drying, grinding, and sieving at room temperature and were finally stored in dark bottles, as illustrated in Fig. 1. Eventually, after shaking their extracts (1:10), the pH and EC of the Ca silicate NPs were measured.
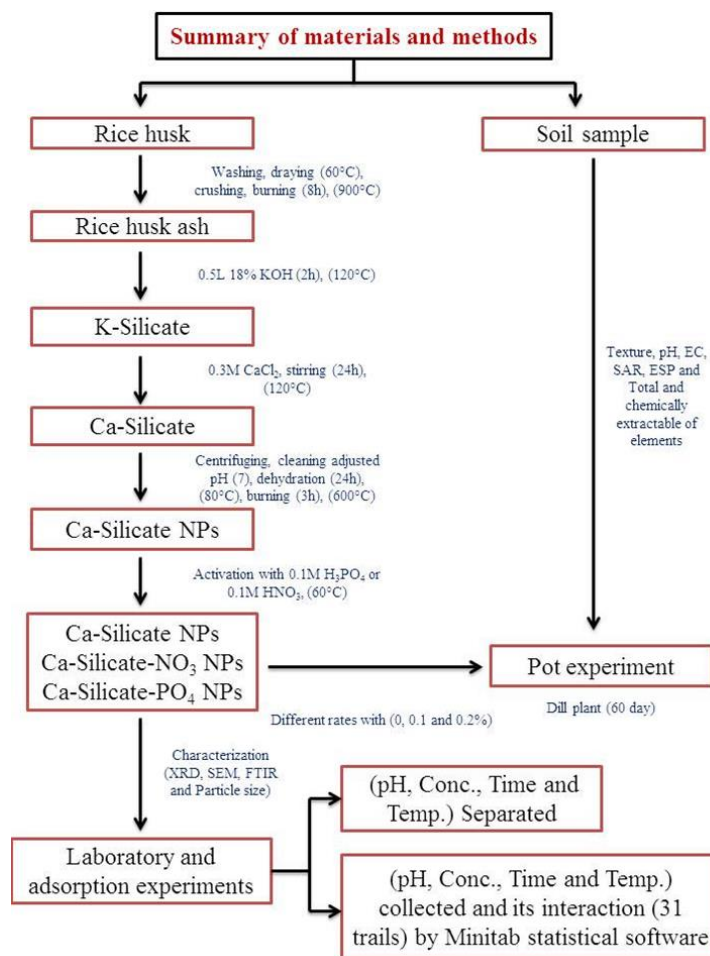
Fig. 1. Schematic view of preparation and application of nanoparticles and their analyses.

2.2.1. Adsorbent characterization

Fourier transform infrared (FTIR) spectroscopy in the wavenumber range of 4000-400 cm^{-1}, utilizing a Nicolet Avatar 230 spectrometer, was used to identify the functional groups of the prepared samples at room temperature. XRD analysis was carried out using (X-ray diffraction Bruker D2 phaser 2nd gen), and the patterns were compared to the Joint Committee on Powder Diffraction Society (JCPDS) database. Scanning electron microscopy (SEM), using (Scanning Electron Microscope Quanta FEG250- FEI- made in USA, Accelerating voltage 20KV), was used to illustrate the surface morphology of samples. Using dynamic light scattering (DLS), utilizing the Malvern Zetasizer Nano-ZS Nano Series, the particle size distribution of Ca silicate, Ca silicate-NO_3, and Ca silicate-PO_4 NPs dispersed in deionized water was determined.

2.3. Adsorption experiments

2.3.1. Effect of concentration

The effect of different concentrations of Na^+ and BO_3^{-3} (20, 50, 100, and 200 ppm) was investigated on the removal percentage (%) using 0.05 g of various Ca silicate NPs. The Ca silicate NPs were put in 10 ml flasks with a volume of 5 ml for each concentration. The source of Na^+ was NaCl, whereas

the BO_3^{-3} was prepared from H_3BO_3. Afterward, the mixtures were mechanically shaken for 6 hours at 350 rpm and a temperature of 298 K to achieve the required equilibrium.

2.3.2. Effect of pH

Na^+ and BO_3^{-3} solutions were investigated at different pH values ranging from 8.1 to 2.09 and 6.08 to 9.5, respectively. A 0.05g of Ca silicate NPs was shaken with 5 ml of 50 ppm of Na^+ and BO_3^{-3} in glass bottles and closed with stoppers for six hours at a constant temperature of 298 K. Subsequently, Na^+ and BO_3^{-3} removal percentages were calculated. The pH adjustment was performed carefully by adding a dilute solution of HCl and NH_4OH.

2.3.3. Effect of temperature

Under constant experimental conditions, the impact of temperature (298, 318, and 338 K) on the adsorption of Na^+ and BO_3^{-3} was investigated. Ca silicate NPs (0.05 g) were added to 5 ml of 50 ppm of Na^+ and BO_3^{-3}, and the mixture was shaken for 6 hours. Finally, the removal percentage (%) was determined.

2.3.4. Effect of contact time

The impact of equilibration time on the removal percentage (%) of Na^+ and BO_3^{-3} was investigated for

various periods ranging from 15 minutes to 96 hours. The experimental condition included 0.05 g of the Ca silicate NPs with the addition of 5 ml of 50 ppm of Na^+ and BO_3^{-3} at a temperature of 298 K.

2.4. Pot experiment

In a pot experiment, the development and yield of the dill plant (*Anethum graveolens* L.) growing in saline soil were examined based on different additives of Ca silicate NPs, Ca silicate-NO_3 NPs, and Ca silicate-PO_4 NPs (0, 0.1, and 0.2% of soil). Each treatment had three replicates; each pot contained 4 kg of soil.

The pots were planted by inserting five seeds of the dill plant (*Anethum graveolens* L.), and after germination, the seedlings were thinned into three plants per pot. Tap water was used as an irrigation source. After 60 days of planting, the dill plant shoots were cut at the soil's surface, washed, oven-dried at 70 °C for 48 hours, and weighed for dry matter yield.

According to Nicholson (1984), after digestion using H_2SO_4-H_2O_2, Na, K, and some trace elements in the shoots were detected. Na and K contents were measured using the flame photometer, whereas BO_3^{-3} was detected using ICPseq-7500. At the end of the pot experiments, soil samples were taken from pots, air-dried, and crushed to fit through a 2 mm sieve, and then pH and EC values were measured.

2.5. Statistical analyses

The data obtained from the pot experiments were analyzed statistically using a computer program (Statistix version 10). Differences between the means of the treatments were considered significant when they exceeded the least significant differences (LSD) at the 5% level.

Response surface methodology (RSM) was used to calculate the maximum Na^+ and BO_3^{-3} removal percentage (%). To maximize the information from the process and minimize the number of potential tests, a central composite design (CCD) was utilized. The multivariate study allows for the identification of interactions between variables.

In this work, the procedure was optimized using a central composite face in which experimental design was performed at three levels (1, 0, and +1) for each factor: pH (A), concentration (ppm) (B), time (h) (C), and temperature (K) (D). For Na^+, the variables pH, concentration (ppm), time (h), and temperature (K) were set to be between (8.1 and 2.09), (20–200 ppm), (0.25–96 h), and (298–338 K), respectively. For boron, the pH was between 6.09 and 9.5. **Table 1** illustrates the levels of coded factors and their actual values. Thirty-one trials were conducted, and Minitab 16 (Minitab® Statistical Software, 2023) was used to formulate the laboratory experiment design.

Table 1. Central composite design of experimental variables (pH, Conc., Time and Temp.).

Trial	coded variables				decoded variables			
	A	**B**	**C**	**D**	**pH**	**Conc. (ppm)**	**Time (h)**	**Temp. (K)**
1	-1	-1	-1	-1	2.9	20	0.25	298
2	1	1	-1	-1	8.1	200	0.25	298
3	-1	1	-1	-1	2.9	200	0.25	298
4	1	1	-1	-1	8.1	200	0.25	298
5	-1	-1	1	-1	2.9	20	96	298
6	1	-1	1	-1	8.1	20	96	298
7	-1	1	1	-1	2.9	200	96	298
8	1	1	1	-1	8.1	200	96	298
9	-1	-1	-1	1	2.9	20	0.25	338
10	1	-1	-1	1	8.1	20	0.25	338
11	-1	1	-1	1	2.9	200	0.25	338
12	1	1	-1	1	8.1	200	0.25	338
13	-1	-1	1	1	2.9	20	96	338
14	1	-1	1	1	8.1	20	96	338
15	-1	1	1	1	2.9	20	96	338
16	1	1	1	1	8.1	200	96	338
17	-1	0	0	0	2.9	200	48.1	318
18	1	0	0	0	8.1	110	48.1	318
19	0	-1	0	0	5.5	110	48.1	318
20	0	1	0	0	5.5	200	48.1	318
21	0	0	-1	-1	5.5	110	0.25	318
22	0	0	1	1	5.5	110	96	318
23	0	0	0	0	5.5	110	48.1	298
24	0	0	0	0	5.5	110	48.1	338
25	0	0	0	0	5.5	110	48.1	318
26	0	0	0	0	5.5	110	48.1	318
27	0	0	0	0	5.5	110	48.1	318
28	0	0	0	0	5.5	110	48.1	318
29	0	0	0	0	5.5	110	48.1	318
30	0	0	0	0	5.5	110	48.1	318
31	0	0	0	0	5.5	110	48.1	318

3. Results

The chemical properties of the collected soil samples from Burg El-Arab, Egypt, considered an industrial, agricultural, and urban area, are listed in Table 2. The pH was 8.01, EC was 5.0 dS.m^{-1}, and ESP was 9.05. The total boron concentration was 99.4 ppm, while the concentration of chemically extractable boron was 0.96 ppm.

3.1. Characterization of NPs

FTIR identifies and investigates the silicate components (Ca silicate NPs, Ca silicate-NO$_3$ NPs, and Ca silicate-PO$_4$ NPs). The bands were seen at ~ 3110 cm^{-1}, between 900 and 1100 cm^{-1}, 1369 and 1415 cm^{-1} in the FTIR chart, as exhibited in Fig. 2.

Table 2. Some physical and chemical properties of the saline soils collected from Burg EL-Arab Egypt.

| Properties	Value	
Particle size distribution (%)		
Sand (%)	80.43	
Silt (%)	10.02	
Clay (%)	9.55	
Texture class	Loamy sand	
OM (%)	0.98	
CaCO$_3$ (%)	28.02	
pH (soil paste extract)	8.01	
EC (dS m^{-1})	5.00	
SAR	7.60	
ESP	9.05	
Elements (ppm)	**Total**	**Available**
B	99.40	0.96
Si	876.00	31.08
Fe	12654.00	106.10
Mn	265.10	13.25
Zn	100.00	2.626
Cu	11.20	0.430
Cr	35.00	0.569
Sr	107.00	1.730
Ni	21.30	0.710
Pb	21.30	0.343
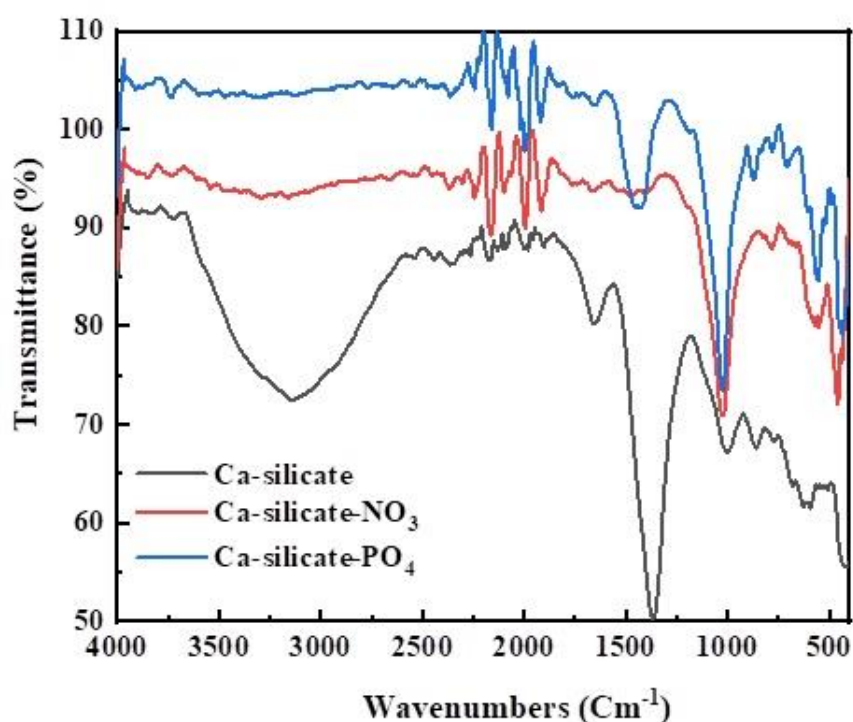
Fig. 2. FTIR patterns of Ca silicate NPs, Ca silicate-NO$_3$ NPs and Ca silicate-PO$_4$ NPs.
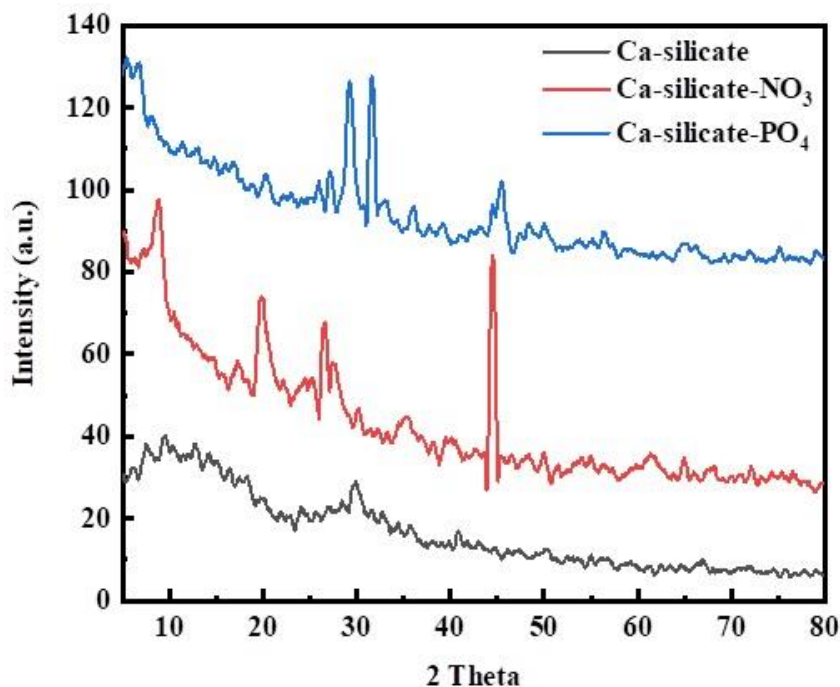
Fig. 3. XRD patterns of Ca silicate, Ca silicate-NO₃ and Ca silicate-PO₄ NPs.

The rice husk was burned at 900°C using a muffle furnace. The XRD analysis was utilized to validate the development of amorphous silica (Ca silicate), as shown in Fig. 3. The XRD pattern displays a distinctive peak at 2θ =29.8°. The pattern of Ca silicate-NO₃ NPs shows different crystalline peaks detected at the equivalent Bragg angle (2θ) at 8.47°, 20.02°, 21.33°, 24.6°, 25.25°, 26.52°, 27.60°, 30.0°, 35.4°, 39.9°, 42.5°, 44.45°, 46.45°, 49.9°, 54.2°, 57.2°, 58.3°, 62.0°, 64.8°, 66.0°, 67.8°, and 72.1°. The emergence of fast peaks demonstrates the presence of crystallinity arrangements in Ca silicate-NO₃ NPs. At the same time, the prepared Ca silicate-PO₄ NPs have different crystalline phases, and the distinctive peaks appeared at 2θ = 4.3°, 5.5°, 6.7°, 8.2°, 12.9°, 14.7°, 16.7°, 20.2°, 25.8°, 27.1°, 29.2°,

31.6°, 33.1°, 36.0°, 54.2°, 39.3°, 42.2°, 44.6°, 45.5°, 47.3°, 48.4°, 50.0°, 53.6°, 55.1°, 56.3°, 62.7°, 66.2°, and 70.5°.

Table 3 shows that all Ca silicate NPs produced under various conditions exhibit high degrees of crystallinity with minimal variation attributed to the different reactions.

As shown in Fig. 4, DLS was used to measure the particle size distributions of Ca silicate NPs, Ca silicate-NO₃ NPs, and Ca silicate-PO₄ NPs. Ca silicate NPs have a particle size of 88.5 nm. Post-treatment with HNO₃ and H₃PO₄ resulted in particle sizes of 87.9 nm and 62.3 nm, respectively, for Ca silicate-NO₃ NPs and Ca silicate-PO₄ NPs.
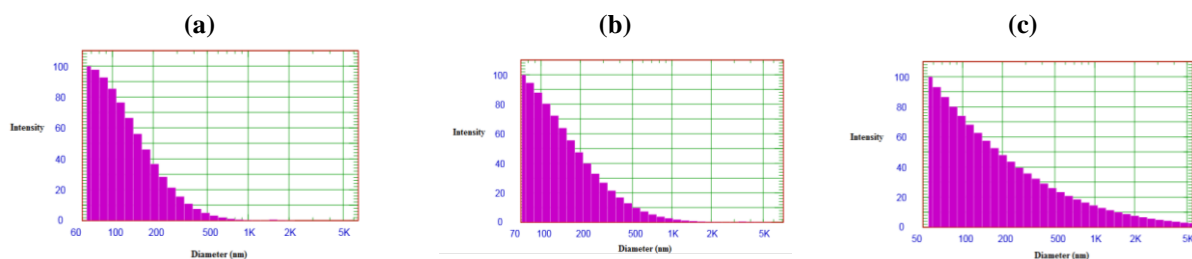

Fig. 4. Particle size distribution of Ca silicate (a), Ca silicate-NO₃ (b) and Ca silicate-PO₄ (c) NPs.

Figure 5 shows SEM microstructures of Ca silicate, Ca silicate-NO₃, and Ca silicate-PO₄ NPs. According to Fig. 5, the surface morphology of Ca silicate NPs showed a proliferation of particles of various sizes. In contrast, Ca silicate-NO₃ NPs and Ca silicate-PO₄ NPs exhibit the development of a thin layer of particles on their surfaces and some coagulation. Acid treatment leads to an increase in particle multiplication, covering more surface area.

When comparing the Ca silicate-PO₄ NPs with the Ca silicate-NO₃ NPs, it was noticed that the surface showed an exemplary distribution of particles but with smaller particle sizes. Additionally, several clusters were noticeable on the surface.

Table 3. XRD data of Ca silicate at different treatment.

| Ca silicate					
Un treated		Activated with HNO$_3$		Activated with H$_3$PO$_4$	
2 θ	d-value(A)°	2 θ	d-value(A)°	2 θ	d-value(A)°
6.1	14.55	8.74	10.11	4.33	20.40
7.7	11.51	20.02	4.43	5.51	16.03
10.0	8.82	21.33	4.16	6.78	13.02
12.7	6.94	24.60	3.61	8.20	10.78
14.6	6.04	25.25	3.52	12.90	6.83
16.4	5.40	26.52	3.35	14.74	6.00
18.2	4.86	27.60	3.22	16.78	5.27
24.0	3.70	30.00	2.93	20.28	4.37
25.9	3.43	35.40	2.53	25.89	3.44
29.8	2.99	39.90	2.25	27.13	3.28
31.8	2.81	42.50	2.12	29.24	3.05
36.0	2.51	44.45	2.03	31.63	2.82
40.8	2.20	46.45	1.95	33.14	2.70
42.7	2.11	49.95	1.82	36.09	2.48
		54.20	1.68	39.33	2.29
		57.20	1.61	42.22	2.14
		58.30	1.58	44.62	2.03
		62.08	1.49	45.59	1.98
		64.87	1.43	47.30	1.92
		66.00	1.41	48.40	1.88
		67.80	1.38	50.03	1.82
		72.14	1.30	53.63	1.70
		74.14	1.27	55.16	1.66
		76.30	1.24	56.35	1.63
		78.20	1.22	62.76	1.48
				66.28	1.41
				70.51	1.33
				75.15	1.26
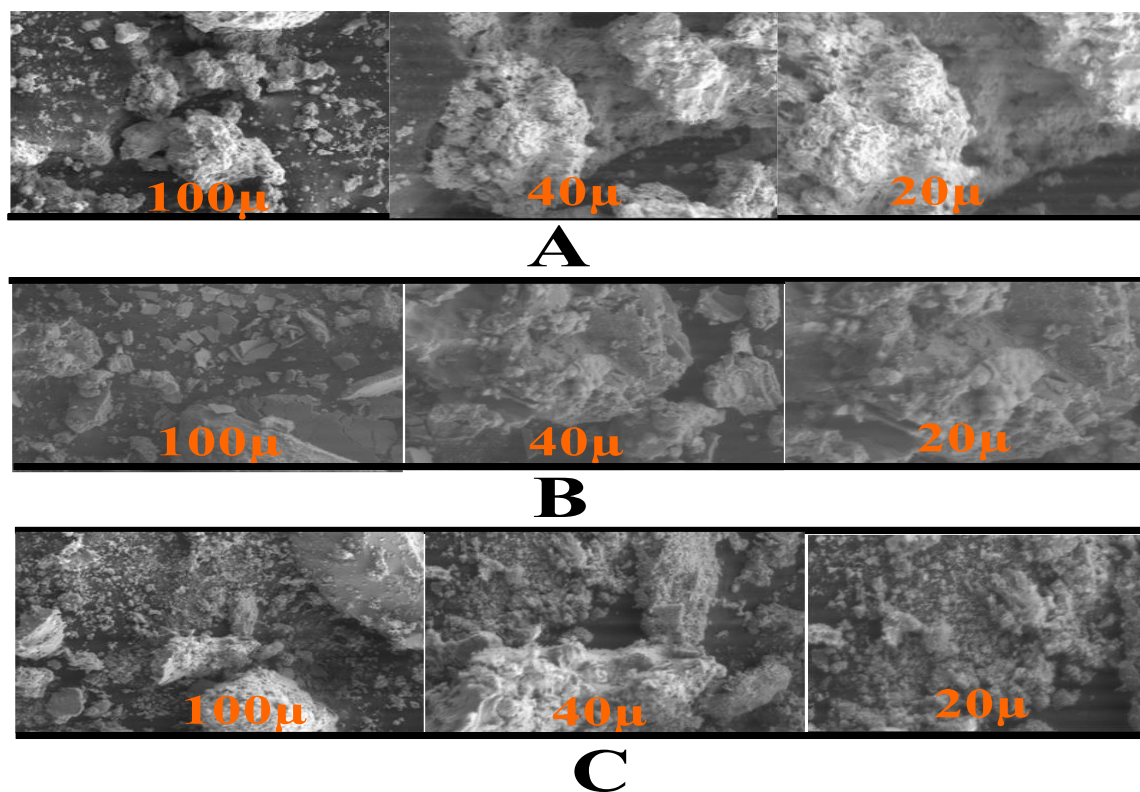
Fig. 5. SEM images of Ca silicate NPs (a), Ca silicate-NO$_3$ NPs (b) and Ca silicate-PO$_4$ NPs (c).

_____

3.2. Adsorption processes
3.2.1. Effect of concentrations

The removal percentages of both Na^+ and BO_3^{-3} were increased in the following order: Ca silicate-PO_4 NPs > Ca silicate-NO_3 NPs > Ca silicate NPs. This trend may be attributed to variations in particle sizes of Ca silicate NPs, Ca silicate-NO_3 NPs, and Ca silicate-PO_4 NPs, which achieved 88.5, 87.9, and 62.3 nm, respectively. In addition, according to the SEM images, Ca silicate-PO_4 NPs possessed a porous structure with a well-pored distribution, indicating the presence of several adsorption sites. This nature makes it an excellent alternative to be utilized in the treatment of water that contains high concentrations of Na^+ and BO_3^{-3}.

The removal efficiency of Na^+ (%) decreased with increasing the initial concentrations using various Ca silicate-NPs as adsorbents, which may be owing to more ions occupying the adsorbent surfaces. The Ca-silicate NPs were treated with Na^+ and BO_3^{-3} at different concentrations from 20 to 50 ppm. The results revealed that the removal efficiencies ranged from 15.72 to 10.88% for Na^+ and 22.36 to 18.98% for BO_3^{-3}. However, at a concentration of 200 ppm, the removal efficiencies declined to 5.39% and 8.29% for Na^+ and BO_3^{-3}, respectively.

It was observed that the activated calcium silicate-PO_4 NPs outperformed the calcium silicate-NO_3 NPs with all concentrations of Na^+ and BO_3^{-3}. Therefore, it can be concluded that the surfaces of calcium silicate-PO_4 NPs are effective for adsorbing cations (e.g., Na^+) and anions (e.g., BO_3^{-3}).

3.2.2. Adsorption isotherms

Langmuir and Freundlich isotherms were utilized to investigate the adsorption of Na^+ and BO_3^{-3} at equilibrium on the surfaces of the sorbents.

The linearized form of the Langmuir equation, presented in Eq. (3), was used to study the Langmuir isotherm for the adsorption of Na^+ and BO_3^{-3}.

$$q_e = \frac{K_L q_m C_e}{1 + K_L C_e} \quad (3)$$

Where q_e is the amount of adsorbate (mg.g^{-1}), and C_e is the adsorbate concentration at equilibrium in solution after adsorption (mg.L^{-1}). The slope and intercept plots of C_e/q_e versus C_e were used to calculate q_m and K_L, where K_L is the Langmuir constant related to adsorption energy, and q_m is the maximum adsorption capacity (mg.g^{-1}). According to the Langmuir equation, specific adsorption results in homogenized adsorption energy without interactions between the adsorbates and neighboring sites.

The heterogeneous multilayer adsorption system is explained using Freundlich isotherms, and its linearized equation is provided as follows (Eq. 4):

log qe = log K_F + 1/n log C_e (4)

Where q_e is the amount of Na^+ or BO_3^{-3} adsorbed at equilibrium (mg g^{-1}). C_e is the equilibrium concentration (mg.L^{-1}), K_F is the Freundlich adsorption constant, and n is the Freundlich exponent. The correlation coefficients for the adsorption capacity determined from the isotherm are shown in Table 4, as well as the Langmuir adsorption constant (K_L) and the constants K_F and n.

Table 4. Estimated isotherm parameters for adsorption of Na^+ and BO_3^{-3} anion on various adsorbents of NPs.

Adsorbate	Adsorbent	Langmiur			Freundlich		
		q_m (mgg^{-1})	K_L	R^2	n	K_F (Lmg^{-1})	R^2
Na^+	Ca silicate- NPs	0.92	0.04	0.73	2.18	0.09	0.69
	Ca silicate-PO_4- NPs	1.63	0.05	0.98	3.08	0.31	0.96
	Ca silicate-NO_3- NPs	1.71	0.01	0.85	1.80	0.08	0.93
Borate	Ca silicate- NPs	1.82	0.02	0.99	2.12	0.14	0.93
	Ca silicate-PO_4- NPs	3.84	0.03	0.98	2.25	0.37	0.88
	Ca silicate-NO_3- NPs	2.56	0.01	0.96	1.96	0.15	0.90

3.2.3. Adsorption kinetics

From the obtained data, the removal percentage of Na^+ and BO_3^{-3} for all the investigated adsorbents increased with increasing the contact time from 0.25 h to 96 h. For Ca-silicate NPs, the removal of Na^+ gradually increased as the contact time increased from 0.25 h to 0.5 h, reaching 4.92%. Subsequently, the removal percentage abruptly elevated by ~ 8.16%, prolonging the time from 0.5 h to 2 h. Further increases of ~10.88% were observed. The removal percentage reached its maximum value at 6 hours and remained constant throughout the reaction time.

The removal percentage (%) of BO_3^{-3} increased abruptly, reaching ~18.89%, as the reaction time increased from 2 to 6 hours. Subsequently, there was a gradual increase of ~18.99%, reaching its maximum value after 72 hours, and it has remained constant for the last 96 hours. The reaction rate was determined using the pseudo-first-order kinetic model. The pseudo-second-order kinetic model can be expressed using Eq. (5), and the adsorption rate constant could be calculated using Eq. (6).

t/q_t = 1/$K_2 q_e^2$ + t/q_e (5)

K_2 represents the pseudo-second-order rate constant (g mg^{-1} min^{-1}), and q_e denotes the equilibrium

_____

Egypt. J. Soil Sci. **64,** No. 1 (2024)

adsorption capacity (mg g^{-1}). These constants were calculated experimentally using the slope and intercept of the plot between t/q_t and t. The intercept of the plot was used to calculate the overall rate constant of the K_2 constant.

Table 5 shows the values of K_1 and qe from plotting a graph of log (q_e-q_t) versus t using equation 6. The

values of K_2 and q_e were also calculated and are listed in Table 5.

$$\log (q_e-q_t) = \log q_e – (K_1/2.303)\ t \quad (6)$$

K_1 represents the adsorption's rate constant (min^{-1}), and q_e and q_t are the concentrations of adsorbate ions (mg g^{-1}) at equilibrium and time t, respectively.

Table 5. Values of parameters calculated from pseudo- first order and pseudo-second order for the removal of Na$^+$ and BO$_3^{-3}$ using different adsorbents of Ca silicate NPs.

Adsorbate	Adsorbent	Pseudo-first order			Pseudo-second order		
		q_e (mg g^{-1})	K_1(min^{-1})	R^2	q_e (mg g^{-1})	K_2 (g mg^{-1} min^{-1})	R^2
Na$^+$	Ca silicate- NPs	0.51	-0.006	0.99	0.706	0.03	1
	Ca silicate-PO$_4$- NPs	0.67	-0.006	0.99	1.179	0.03	1
	Ca silicate-NO$_3$- NPs	0.54	-0.002	0.96	0.95	0.01	0.99
BO$_3^{-3}$	Ca silicate- NPs	0.67	-0.002	0.76	1.13	0.02	0.99
	Ca silicate-PO$_4$- NPs	1.52	-0.009	0.99	2.53	0.01	1
	Ca silicate-NO$_3$- NPs	0.31	-0.004	0.77	1.53	0.08	1

3.2.4. Effect of solution pH

Ca silicate NPs (0.05 g) were added to 5 ml of Na$^+$ solutions with a pH ranging from 2.09 to 8.1 and stirred for 6 hours to evaluate the impact of pH. The

Na$^+$ removal percentage (%) increased from 5.62 to 10.20%, with the pH increasing from 2.09 to 8.1, as presented in Fig. 6.
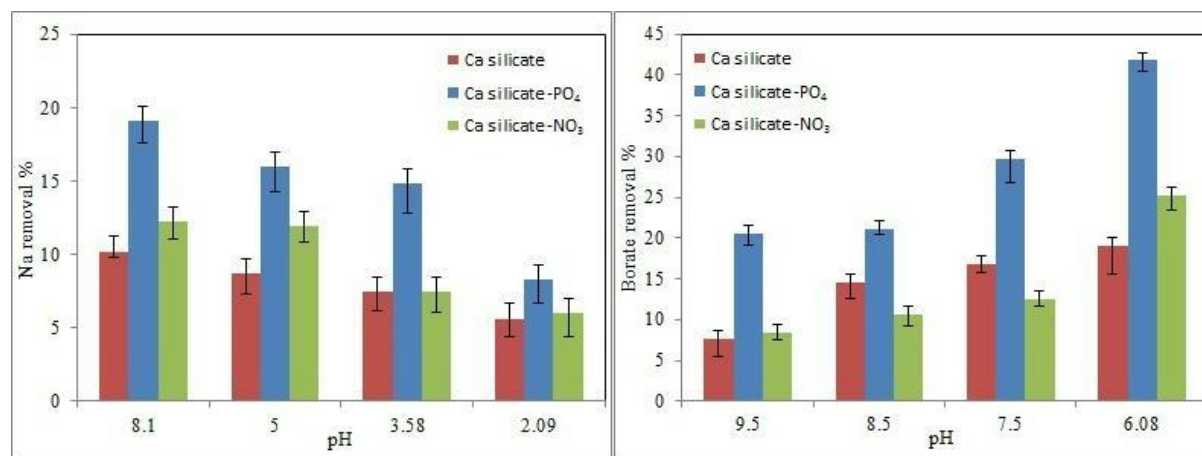
Fig. 6. Effects of adsorption at different pH values on removal of Na$^+$ and BO$_3^{-3}$ (b) using different adsorbents of calcium silicate NPs.

3.2.5. Thermodynamics of the adsorption process

The thermodynamic parameters, presented in Table 6, were calculated with temperature conditions ranging from 298 K to 338 K for adsorption experiments while keeping other variables constant. The thermodynamic parameters of ΔG°, ΔH°, and ΔS° were computed using the thermodynamic equations (7, 8, and 9) below. These parameters describe the removal percentage of Na$^+$ and BO$_3^{-3}$ using the investigated adsorbents. The adsorption study, at equilibrium, can be considered a heterogeneous, reversible process. The standard

Gibbs free energy change for the adsorption, ΔG°, was determined, and the universal gas constant was set to be R (8.314 J mol^{-1} K^{-1}).

$$K_c = C_{ad} / C_e \quad (7)$$
$$\Delta G° = - R\ T \ln K_c \quad (8)$$
$$\Delta G° = \Delta H° –T\ \Delta S° \quad (9)$$

Where – ΔS° denotes the straight line with a slope, and ΔH° represents the intercept of results. These values can be obtained from the plot of T versus ΔG°. The exothermic nature of the procedure employed for removing Na$^+$ and the BO$_3^{-3}$ is indicated by the negative value of ΔH°; see Table 6.

Table 6. Thermodynamic parameters using different adsorbents of Ca silicate NPs, Na$^+$ and borate anion solution of 50 ppm.

adsorbate	adsorbent	T (K)	ΔG_o	ΔH_o	ΔS_o
	Ca silicate NPs	298	5209.4		
		318	5286.7	9.393	2373.5
		338	5586.1		
Na$^+$	Ca silicate-PO$_4$ NPs	298	3585.4		
		318	3673.7	7.580	1305.3
		338	3888.6		
	Ca silicate-NO$_3$ NPs	298	4879.6		
		318	5201.2	-5.22	6578
		338	4670.72		
	Ca silicate NPs	298	4501.6		
		318	4195.9	-10.58	7623.5
		338	4078.3		
borate	Ca silicate-PO$_4$ NPs	298	3614.2		
		318	2242.6	-67.01	23574
		338	933.6		
	Ca silicate-NO$_3$ NPs	298	4388.1		
		318	4052.2	-33.38	14447
		338	3052.7		

3.3. Parameter optimization

After conducting the 31 trials in the studied area, the studied parameters were optimized through the application of a multivariate design. The pH, concentrations, contact time, and temperature were selected as the variables or components for the study due to their significant impact on the adsorption process. Table 7 lists the expected and experimental results for Ca silicate NPs, Ca silicate-NO$_3$ NPs, and Ca silicate-PO$_4$ NPs, detailing their effectiveness in removing Na$^+$ and BO$_3^{-3}$, along with corresponding R^2 and R^2_{adj} values.

Table 7. The expected and experimental results for the sorbents of Ca silicate NPs, Ca silicate-NO$_3$ NPs, and Ca silicate-PO$_4$.

Trial	Ca silicate NPs				Ca silicate- PO$_4$ NPs				Ca silicate-NO$_3$ NPs			
	Na		Borate		Na		Borate		Na		Borate	
	O[1]	P[2]	O	P	O	P	O	P	O	P	O	P
1	4.52	5.26	22.30	18.47	11.51	12.43	42.10	36.91	7.91	7.35	25.20	24.70
2	18.84	14.98	6.10	7.62	32.40	28.39	18.20	17.28	15.20	12.26	7.20	7.15
3	3.48	2.28	6.40	10.28	7.21	5.89	18.30	24.45	4.08	5.10	16.70	18.01
4	3.55	7.54	7.50	5.78	8.26	13.54	18.90	16.52	4.30	6.08	8.01	8.67
5	17.64	16.50	20.10	21.96	30.08	28.35	39.40	42.74	12.05	12.32	25.50	27.73
6	20.04	23.29	9.70	8.96	33.65	36.86	22.30	21.41	16.05	18.78	10.50	8.93
7	7.96	9.93	16.30	14.17	10.39	13.98	35.20	29.44	8.05	6.96	21.10	20.09
8	15.16	12.25	8.20	7.52	18.75	14.17	21.30	19.81	10.68	9.50	9.20	9.49
9	3.95	4.82	12.30	16.40	8.39	11.38	26.20	32.07	7.50	7.61	22.90	22.87
10	12.04	12.74	9.10	7.45	28.08	26.33	16.20	16.79	8.12	10.06	10.30	10.72
11	8.48	7.90	12.30	9.26	13.28	11.91	25.20	20.91	11.61	9.72	15.40	16.38
12	12.24	11.35	5.10	6.66	18.40	18.54	16.30	17.33	9.60	8.25	14.40	12.43
13	18.80	17.48	22.90	20.84	32.05	28.61	41.40	38.60	14.80	13.87	25.50	24.25
14	23.28	22.46	10.20	9.74	36.36	36.09	23.40	21.62	19.96	17.87	11.90	10.84
15	15.12	16.96	12.20	14.10	18.88	21.30	21.30	26.60	11.00	12.87	16.50	16.81
16	15.56	17.48	9.30	9.35	19.55	20.47	21.30	21.32	11.55	12.95	11.70	11.60
17	8.12	6.94	18.30	17.64	15.80	13.74	41.20	38.57	7.58	8.80	25.20	23.16
18	13.44	12.06	7.70	9.84	20.24	21.31	20.30	26.12	11.56	11.29	8.40	11.78
19	12.27	13.85	14.40	15.68	19.95	24.04	26.20	27.98	11.92	13.41	10.20	12.00
20	14.01	9.87	11.20	11.39	18.04	12.97	20.20	21.61	10.36	9.82	9.50	9.04
21	4.72	4.94	17.40	16.59	11.88	11.01	32.20	31.34	4.77	6.69	19.60	18.77

1: Observed   2: Predicted

Table 7. Cont.

Trial	Ca silicate NPs				Ca silicate- PO$_4$ NPs				Ca silicate-NO$_3$ NPs			
	Na		Borate		Na		Borate		Na		Borate	
	O[1]	P[2]	O	P	O	P	O	P	O	P	O	P
22	16.40	13.62	17.40	19.68	20.05	19.93	32.20	36.25	12.49	11.52	17.70	19.87
23	12.24	11.39	14.30	16.15	19.04	17.69	20.20	27.33	11.08	11.06	16.20	14.85
24	15.48	13.78	16.40	16.02	19.94	20.31	29.60	25.66	11.96	12.92	12.30	14.99
25	9.08	10.18	17.20	16.57	16.24	16.66	32.10	30.73	11.08	10.68	16.10	15.52
26	9.08	10.18	17.20	16.57	16.24	16.66	32.10	30.73	11.08	10.68	16.10	15.52
27	9.08	10.18	17.20	16.57	16.24	16.66	32.10	30.73	11.08	10.68	16.10	15.52
28	9.08	10.18	17.20	16.57	16.24	16.66	32.10	30.73	11.08	10.68	16.10	15.52
29	9.08	10.18	17.20	16.57	16.24	16.66	32.10	30.73	11.08	10.68	16.10	15.52
30	9.08	10.18	17.20	16.57	16.24	16.66	32.10	30.73	11.08	10.68	16.10	15.52
31	9.08	10.18	17.20	16.57	16.24	16.66	32.10	30.73	11.08	10.68	16.10	15.52
R^2 (%)	86.13		85.80		89.65		80.48		83.45		93.73	
R^2_{adj} (%)	73.99		73.38		80.59		63.40		68.96		88.24	

1: Observed   2: Predicted

3.4. Analysis of variance (ANOVA)

The analysis of variance (ANOVA) is employed to evaluate the statistical significance of the model and the variability in the number of components influencing the adsorption capacity of Ca silicate for each factor. This assessment considers interactions and experimental error simultaneously. The significance can be determined by examining the F ratio and corresponding p-values.

The ANOVA results for the removal of Na$^+$ and BO_3^{-3} using calcium silicate NPs, calcium silicate-NO$_3$ NPs, and calcium silicate-PO$_4$ NPs are presented in Table 8. The results demonstrate significant effects, as indicated by large F ratios, for pH and concentration factors, with corresponding p-values less than 0.05. A mathematical relationship, derived from the Minitab statistical software, can be used to characterize the quantitative impacts of process variables such as pH, concentration, contact time, and temperature and their interactions based on the observed response (removal percent (%) of Na$^+$ and BO_3^{-3}). Upon disregarding p-values greater than 0.05 (refer to Table 8), the mathematical correlations established a connection between the observed response (removal percentage) and model variables. This connection can be defined by the regression equations (10 to 15) produced by the Minitab statistical software, as listed in Table 9.

Table 8. ANOVA for the removed Na$^+$ and BO_3^{-3} different adsorbent of Ca silicate NPs.

Source	Ca silicate NPs				Ca silicate- PO$_4$ NPs				Ca silicate-NO$_3$ NPs			
	Na$^+$		BO_3^{-3}		Na$^+$		BO_3^{-3}		Na$^+$		BO_3^{-3}	
	F ratio	p value	F ratio	p value	F ratio	p value	F ratio	p value	F ratio	p value	F ratio	p value
pH	16.91	0.00	42.89	0.00	23.14	0.00	31.51	0.00	8.30	0.01	170.5	0.00
Conc. (ppm)	10.22	0.00	12.97	0.00	49.58	0.00	8.26	0.01	17.17	0.00	11.59	0.00
Time (h)	48.64	0.00	6.73	0.02	32.20	0.00	4.90	0.04	31.22	0.00	1.59	0.22
Temp. (K)	3.69	0.07	0.01	0.92	2.79	0.11	0.56	0.46	4.60	0.04	0.03	0.87
pH*Conc.	2.85	0.11	6.32	0.02	6.21	0.02	8.18	0.02	4.56	0.04	19.70	0.00
pH*time	1.24	0.28	0.72	0.40	5.00	0.04	0.13	0.72	0.72	0.41	0.46	0.50
pH*Temp.	0.47	0.50	0.57	0.46	0.09	0.76	0.85	0.36	1.79	0.19	8.53	0.01
Conc. *time	1.85	0.19	0.03	0.87	5.51	0.03	0.03	0.85	2.89	0.11	0.27	0.61
Conc. *Temp.	5.26	0.03	0.17	0.68	4.48	0.05	0.08	0.78	5.66	0.03	0.01	0.91
Time*Temp.	0.29	0.60	0.14	0.71	0.15	0.70	0.02	0.88	0.49	0.49	0.79	0.38

_____

Table 9. Regression equations for the removal of Na$^+$ and BO$_3^{-3}$ using different adsorbents of Ca silicate NPs.

Removal % of Na$^+$ by calcium silicate NPs	= 602.52+5.64pH-0.29Conc.+ 0.06time+ 0.00084Conc.*Temp.	(10)
Removal % of Na$^+$ by calcium silicate–PO$_4$ NPs	=605.58+3.30pH-0.35Conc.+0.16time-0.008pH*Conc.-0.01pH*time-0.0004Conc.*time+0.0009Conc.*temp.	(11)
Removal % of Na$^+$ by calcium silicate –NO$_3$ NPs	=325.34+5.57pH-0.20Conc.+0.01time-2.06Temp.-0.004pH*Conc.+0.0006Conc.Temp.	(12)
Removal % of BO$_3^{-3}$ by calcium silicate NPs	=-97.98+7.58pH-0.06Conc.-0.06time+0.01pH*Conc.	(13)
Removal % of BO$_3^{-3}$ by calcium silicate–PO$_4$ NPs	=-867.43-24.19pH-0.07Conc.-0.08time+0.01pH*Conc.	(14)
Removal % of BO$_3^{-3}$ by calcium silicate –NO$_3$ NPs	=28.01-7.53pH+0.009Conc.+0.01pH*Conc.+0.03pH*Temp.	(15)

3.5. Plots of residuals versus predictions

Figure 7 (a and b) shows a random distribution of residuals along the reference line. The amplitude of these residuals fluctuated from up to down along the zero line, indicating that the experimental errors continuously vary with the mean response.

(a)   (b)
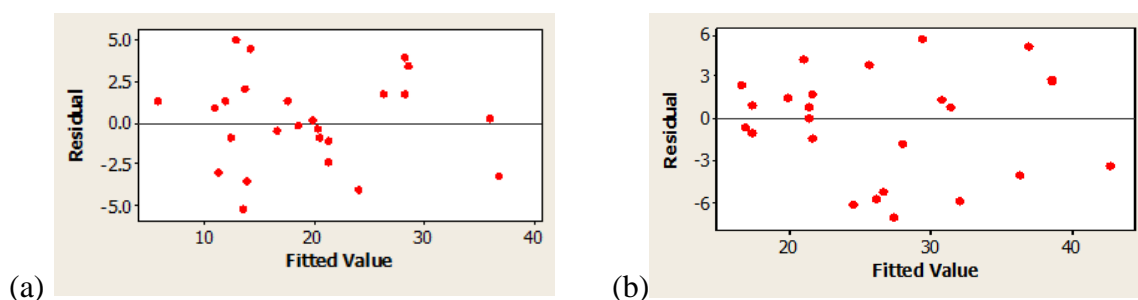
Fig. 7. Random distribution of residuals for removed of Na$^+$ (%) (a), and BO$_3^{-3}$ (%) (b) using Ca silicate-PO$_4$ NPs.

3.6. Surface plots of response

The predicted responses of the variables (removal percentage, %) of Na and BO$_3^{-3}$ by Ca silicate NPs, Ca silicate-NO$_3$ NPs, and Ca silicate-PO$_4$ NPs were examined based on response surface plots. The interactive effects of parameters, including pH, concentrations, contact time, and temperature, on the removal percentage (%) of Na$^+$ and BO$_3^{-3}$ by Ca silicate-PO$_4$ NPs are depicted in Figures 8 and 9. Figures 8 and 9 demonstrate the expected response charting of Na$^+$ and BO$_3^{-3}$ removal percentage (%) by Ca silicate-PO$_4$ NPs against two of the four studied parameters (pH, concentrations, contact time, and temperature), while the other two parameters were set at the medium values (hold values). The diagram surface's height value determines the removal percentage's expected response (%). By comparing the various Ca silicate NPs, it was found that Ca silicate-PO$_4$ NPs have the largest surface area during reactions. Fig. 8(a) demonstrates the reciprocal relationship between pH and concentration. The removal percentage gradually increases as pH rises and Na$^+$ ion concentration decreases. Furthermore,

Fig. 8(b) depicts the combined impact of pH and contact time, wherein the removal percentages increase as pH is elevated and contact time is prolonged. Fig. 8(c) illustrates the combined impact of pH and temperature; the removal percentage increases when both pH and temperature increase. Fig. 8(d) illustrates the interaction between concentrations and contact time; the removal percentage gradually increases as concentrations and contact time are reduced. Fig. 8(e) shows the interaction between concentrations and temperature, displaying a curving relationship wherein temperature decreases as concentrations increase. In Fig. 8(f), the combined impact of contact time and temperature is depicted, demonstrating a rapid increase in removal percentages as contact time and temperature are prolonged and decreased, respectively. Fig. 8(e) displays the interactive effect of concentrations and temperature, revealing a curved relationship in the removal percent (%) with both concentrations and temperature. Fig. 8(f) shows the combined effect of contact time and temperature, indicating a slow increase in removal percent (%)

_____

with increasing contact time, while temperature exhibited a curved relationship.

Figure 9(a) demonstrates the interaction between pH and concentrations. While concentrations exhibit a curved relationship with pH, the removal percentage of BO_3^{-3} drops as pH increases. Figure 9(b) illustrates the interaction between pH and contact time, revealing a rapid decrease in removal percentages as pH and shaking duration increase. Figure 9(c) demonstrates the interaction between pH and temperature; although temperature has a curved relationship with pH, the removal percentage drops as pH increases. Figure 9(d) demonstrates the interaction between concentrations and contact time. The removal percentage of BO_3^{-3} progressively increases as contact time is extended, but concentrations exhibit a curved relationship. The removal percentage demonstrates a curving relationship with both concentrations and temperature, as shown in Figure 9(e), illustrating the interacting effect of concentrations and temperature. the removal percentage of BO_3^{-3} has a curved relationship with concentrations and temperature.

Figure 9(f) shows the combined effect of contact time and temperature; the removal percentage of BO_3^{-3} slowly increases with increasing contact time, while temperature exhibits a curved relationship.

3.7. Optimized responses

Table 10 lists the anticipated optimum conditions (pH, concentrations, contact time, and temperature) for the removal of Na^+ and BO_3^{-3}. It indicates the maximum removal percentages (%) achieved by the various adsorbents of Ca silicate NPs, reaching their highest values.

3.8. Effects of application Ca silicate NPs on some soil properties and dill plant productivity

After the treatment with Ca silicate NPs, Ca silicate-NO_3 NPs, and Ca silicate-PO_4 NPs, significant effects were observed on the uptake of some elements such as Na, Ca, B, Si, Al, and Mn in dill plants, as illustrated in Table 11. However, in the fresh and dry weight of the dill plant, the contents of some elements such as Fe, Zn, Cr, and Sr, as well as the pH and EC of the soil, were not significantly affected by various adsorbents of Ca silicate NPs.

(a)

(b)

(c)

(d)

(e)

(f)
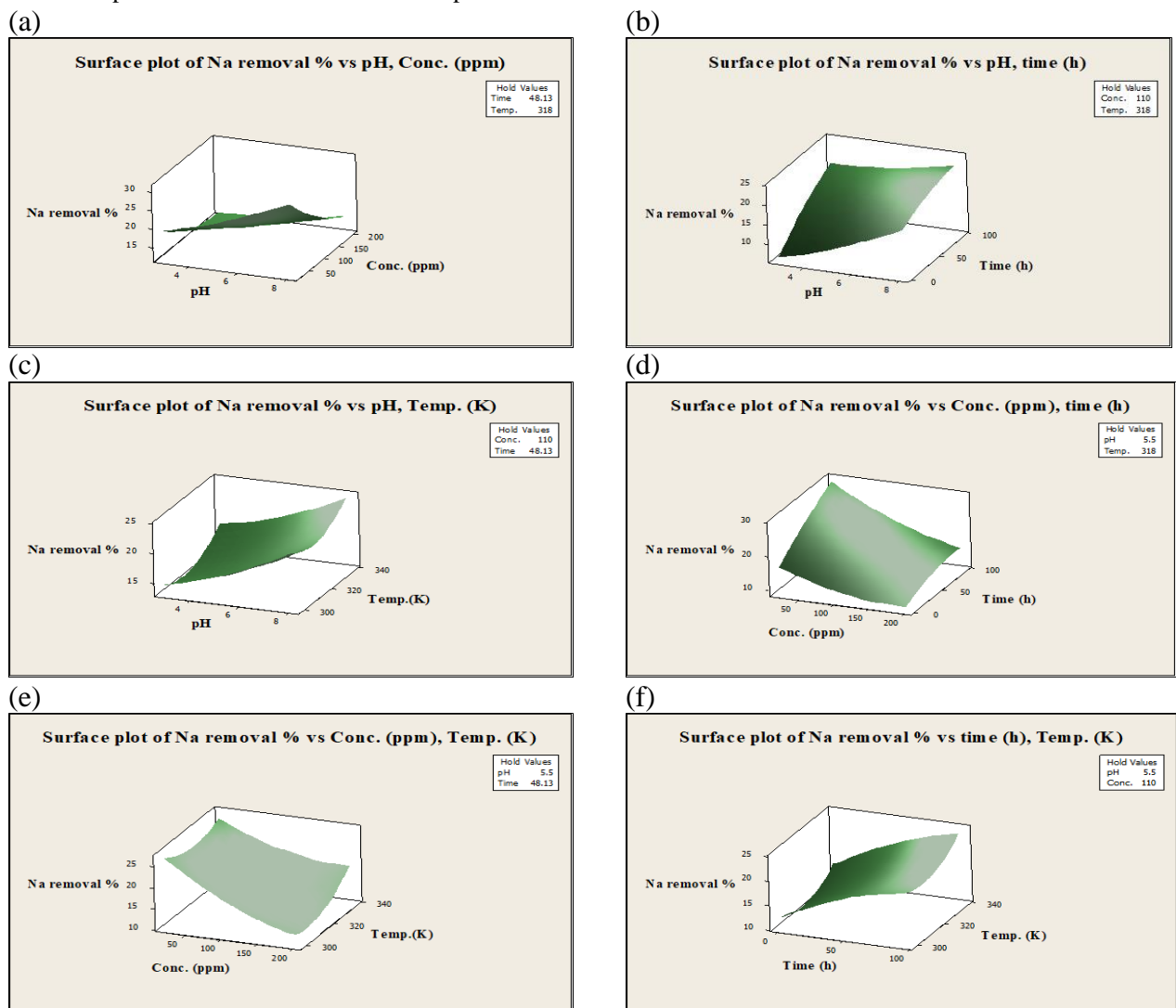
Fig. 8. (a–f) The response surface plots for the removal of Na^+ by using Ca silicate-PO_4 NPs.

(a)

(b)

(c)

(d)

(e)

(f)
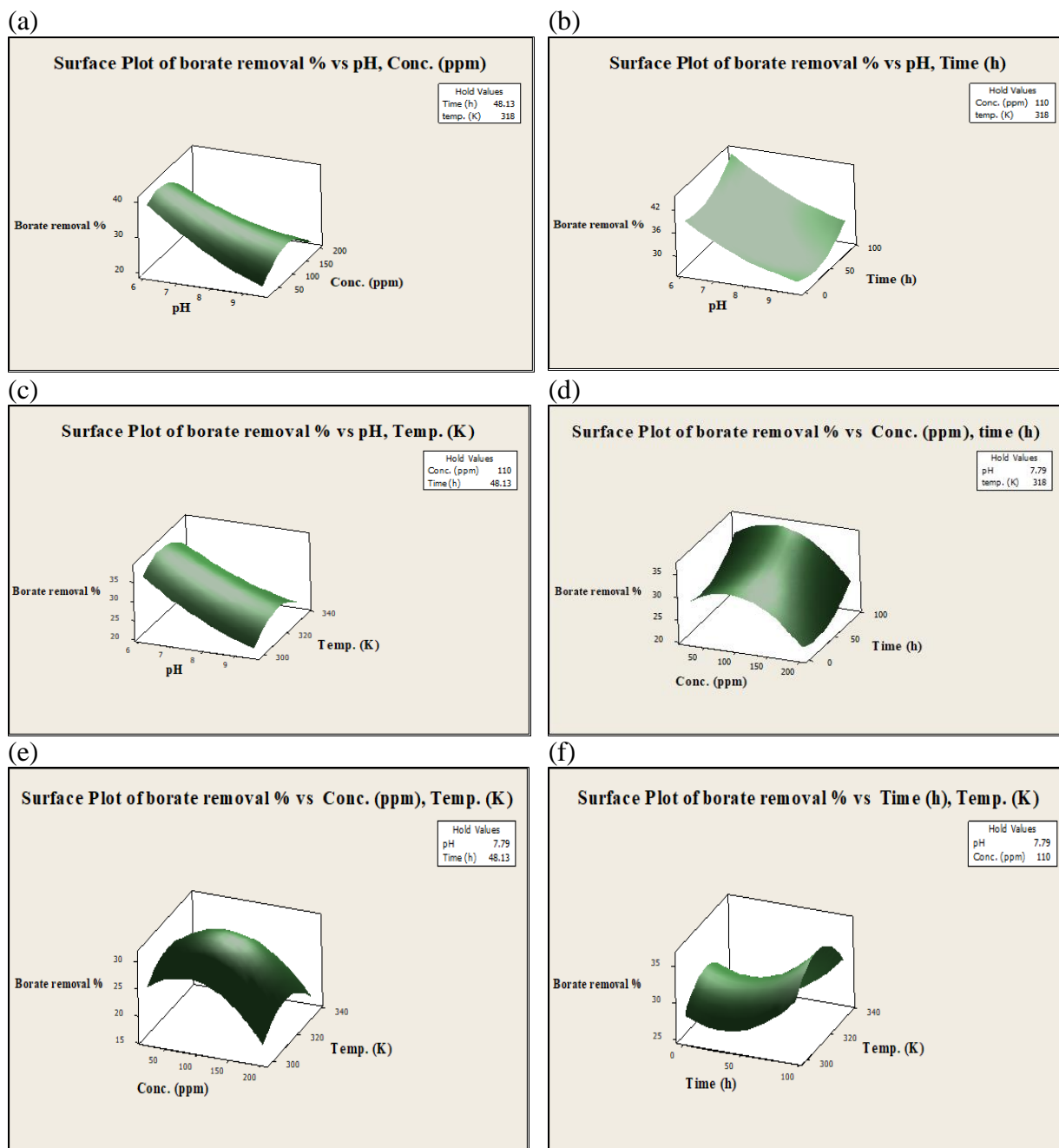
Fig. 9. (a–f) The response surface plots for the removal of BO_3^{-3} by using Ca silicate-PO$_4$ NPs.

Table 10. The anticipated optimum conditions (pH, concentration, time, and temperature) for the removal of Na$^+$ and BO_3^{-3}.

The removed elements & Adsorbents	pH	Conc. (ppm)	Time (h)	Temp. (K)	Optimized responses (removal %)
Removal % of Na$^+$ by Ca silicate NPs	8.10	20	96	298	18.78
Removal % of Na$^+$ by Ca silicate-PO$_4$ NPs	8.10	20	96	298	36.85
Removal % of Na$^+$ by Ca silicate-NO$_3$ NPs	8.10	20	96	298	23.28
Removal % of BO_3^{-3} by Ca silicate NPs	6.08	54.54	96	308.5	22.47
removal % of BO_3^{-3} by Ca silicate -PO$_4$ NPs	6.08	61.81	96	313.3	46.42
removal % of BO_3^{-3} by Ca silicate-NO$_3$ NPs	6.08	76.36	96	298	29.63

Table 11. Effect of different amendments on pH, EC in soil and content of some elements in Dill plant.

Amendments / Rates	pH				EC (dS/m)			
	Ca Silicate -PO₄	Ca Silicate -NO₃	Ca Silicate	Means (Rate)	Ca Silicate -PO₄	Ca Silicate -NO₃	Ca Silicate	Means (Rate)
Control	7.80C	7.80C	7.80C	7.80C	4.44A	4.44A	4.44A	4.44A
0.1%	7.97AB	7.96B	7.99AB	7.97B	4.20AB	4.31A	4.30A	4.27B
0.2%	8.04AB	8.10A	8.06AB	8.07A	3.93B	4.16AB	4.16AB	5.08C
Means (A)	7.93A	7.95A	7.95A		4.19A	4.30A	4.30A	
L.S.D. at 0.05% for	A= 0.11	Rate=0.07	A*R=0.15		A= 0.14	Rate=0.16	A*R=0.27	

Amendments / Rates	fresh weight (g/pot)				dry weight (g/pot)			
	Ca Silicate -PO₄	Ca Silicate -NO₃	Ca Silicate	Means (Rate)	Ca Silicate -PO₄	Ca Silicate -NO₃	Ca Silicate	Means (Rate)
Control	3.30CD	3.30CD	3.30D	3.3B	1.60BC	1.9BC	1.63BC	1.73A
0.1%	4.13AB	4.76A	3.50BCD	4.13A	1.83BC	2.60A	1.66BC	2.03A
0.2%	3.56BCD	4.16AB	3.96BC	3.90A	1.56C	2.30AB	2.20ABC	2.02A
Means (A)	3.66A	4.07A	3.58A		1.66B	2.28A	1.83AB	
L.S.D. at 0.05% for	A= 0.54	Rate= 0.36	A*R=0.73		A= 0.52	Rate= 0.35	A*R= 0.71	

Amendments / Rates	Na (meq/g.dw)				Ca (meq/g.dw)			
	Ca Silicate -PO₄	Ca Silicate -NO₃	Ca Silicate	Means (Rate)	Ca Silicate -PO₄	Ca Silicate -NO₃	Ca Silicate	Means (Rate)
Control	1.195A	1.19A	1.19A	1.19A	1.05E	1.05E	1.05E	1.05C
0.1%	0.48F	0.77D	0.89B	0.71B	1.37AB	1.26BC	1.12DE	1.25B
0.2%	0.34G	0.66E	0.82C	0.61C	1.47A	1.28BC	1.22CD	1.32A
Means (A)	0.67C	0.87B	0.97A		1.29A	1.20B	1.13B	
L.S.D. at 0.05% for	A= 0.03	Rate= 0.02	A*R= 0.04		A= 0.08	Rate= 0.05	A*R= 0.11	

Amendments / Rates	B (ppm)				Si (ppm)			
	Ca Silicate -PO₄	Ca Silicate -NO₃	Ca Silicate	Means (Rate)	Ca Silicate -PO₄	Ca Silicate -NO₃	Ca Silicate	Means (Rate)
Control	45.31A	45.31A	45.31A	45.31A	4480.1G	4480.1G	4480.1G	4480.1C
0.1%	31.61D	35.21C	39.60B	35.47B	6093.3B	5692.6E	5595.3F	5793.7B
0.2%	21.61F	25.65E	30.91D	26.06C	6358.3A	5903.4C	5789.6D	6017.1A
Means (A)	32.84C	35.39B	38.60A		5643.9A	5358.7B	5288.3C	
L.S.D. at 0.05% for	A= 0.78	Rate= 2.17	3.17		A=28.37	Rate= 25.03	A*R= 45.07	

Amendments / Rates	Fe (ppm)				Mn (ppm)			
	Ca Silicate -PO₄	Ca Silicate -NO₃	Ca Silicate	Means (Rate)	Ca Silicate -PO₄	Ca Silicate -NO₃	Ca Silicate	Means (Rate)
Control	4181.0B	4181.0B	4181.0B	4181.0A	106.30A	106.30A	106.30A	106.3A
0.1%	2697.6D	3962.4B	4506.3A	3722.1B	69.33C	97.80B	106.0A	91.04B
0.2%	2753.7D	1721.8E	3531.2C	2668.9C	60.89D	73.00C	98.53B	77.4C
Means (A)	3210.8B	3288.4B	4072.8A		78.84C	92.37B	103.6A	
L.S.D. at 0.05% for	A=140.1	Rate= 136.0	A*R=167.6		A= 5.16	Rate=3.98	A*R= 7.59	

Amendments / Rates	Zn (ppm)				Cr (ppm)			
	Ca Silicate -PO₄	Ca Silicate -NO₃	Ca Silicate	Means (Rate)	Ca Silicate -PO₄	Ca Silicate -NO₃	Ca Silicate	Means (Rate)
Control	96.49AB	96.4AB	96.4AB	96.4A	17.0B	17.0B	17.0B	17.0B
0.1%	1023A	72.0D	94.6ABC	89.6B	29.0AB	32.0AB	28.6AB	29.8A
0.2%	!01.0A	87.3C	88.3BC	92.2B	35.0A	32.0AB	27.0AB	31.3A
Means (A)	99.9A	85.2B	93.1A		27.0A	27.0A	24.2A	
L.S.D. at 0.05% for	A= 6.85	Rate=4.24	A*R=236.60		A= 6.49	Rate=10.18	A*R= 15.73	

Amendments / Rates	Al (ppm)				Sr (ppm)			
	Ca Silicate -PO₄	Ca Silicate -NO₃	Ca Silicate	Means (Rate)	Ca Silicate -PO₄	Ca Silicate -NO₃	Ca Silicate	Means (Rate)
Control	3374.0B	3374.0B	3374.0B	3374.0A	215.67E	215.6E	215.6E	215.6C
0.1%	2236.7D	2972.3C	3705.3A	29711.4B	293.7C	296.9B	260.9D	283.8B
0.2%	2280.7D	2983.3C	2712.7C	2658.9C	327.5A	322.13A	285.6C	311.7A
Means (A)	2630.4C	3109.9B	3264.0A		280.0A	277.1A	254.0B	
L.S.D. at 0.05% for	A=153.5	Rate=167.6	A*R= 280.97		A= 3.8	Rate=5.3	A*R=8.4	

3.9. Comparison of removal of Na$^+$ and BO$_3^{-3}$ by some different adsorbents

Table 12 compares the removal percentages of Na$^+$ and BO$_3^{-3}$ by various adsorbents in the present study with other relevant literature. In our investigation, the removal percentage of Na$^+$ and BO$_3^{-3}$ by Ca silicate NPs reached 15.72 and 22.36%, respectively.

Table 12. Comparison of some different adsorbents for removed Na$^+$ and BO_3^{-3}.

The removed elements	Adsorbents	Capacity	Reference
BO$_3^{-3}$	Ca silicate NPs	22.36%	The present work
	Ca silicate-PO$_4$ NPs	43.98%	The present work
	Ca silicate-NO$_3$ NPs	25.99%	The present work
	Amberlite™ (PWA10 Macroporous polystyrene)	≥0.7 eq l^{-1}	Hilal et al. (2011)
	IRA743 (Macroporous polystyrene)	0.7 eq l^{-1}	Hilal et al. (2011)
	Diaion (CRB01 Macroporous polystyrene-DVB)	≥1.2 eq l^{-1}	Hilal et al. (2011)
	CRB02 (Macroporous polystyrene-DVB)	≥0.9 eq l^{-1}	Hilal et al. (2011)
	Dowex™ (BSR-1 Macroporous polystyrene-DVB)	0.7 eq l^{-1}	Hilal et al. (2011)
	Purolite (S108 Macroporous polystyrene-DVB)	0.6 eq l^{-1}	Hilal et al. (2011)
	S110 (Macroporous polystyrene-DVB)	0.8 eq l^{-1}	Hilal et al. (2011)
	Uncalcined Mg–Al LDHs	14 mg g^{-1}	Ferreira et al. (2005)
	Uncalcined nitrate-Mg–Al LDHs	20 mg g^{-1}	Ay et al. (2007)
	Uncalcined LDHs	20 mg g^{-1}	You et al. (2001)
	Mg–Al- MAA LDH	5 mg g^{-1}	Soliman et al. (2019)
Na$^+$	Natural bentonite	22.5%	Musie and Gonfa (2022)
	Activated nano bentonite	24%	Musie and Gonfa (2022)
	Zeolite (clinoptilolite)	1000 (q$_{max}$)(mg g^{-1})	Shokrian et al. (2015)
	Bentonite (depend on kind of anion)	(66-115) meq 100g^{-1}	Sommerfeldt (1961)
	fique fibers (Furcraea spp.)	15.52 mg g^{-1}	Agudelo et al. (2016)
	Nanometer Calcium Silicate Channel	Capillary method	Hou et al. (2017)
	Ca silicate NPs	15.72%	The present work
	Ca silicate-PO$_4$ NPs	33.18%	The present work
	Ca silicate-NO$_3$ NPs	19.21%	The present work
Sodium leucovat-dye	Acid activated natural clay	88%	Chaari et al. (2020)

4. Discussions

The results indicating that Burg El-Arab is considered an industrial, agricultural, and urban area (with more than 459 factories) are listed in Table 2. The pH was 8.01, EC was 5.0 dS m^{-1}, and ESP was 9.05, indicating soils fall within the category of saline soils. The total boron concentration was 99.4 ppm, which is more than the maximum level of boron in soil (Brdar-Jokanović, 2020).

The FTIR spectrum (Figure 2) reveals chemically or physically absorbed water (Pavia et al., 2009). The O-Si-O bond exhibits bands near 750 to 900 cm^{-1}. These bands demonstrate the presence of silicates in the samples. Bands between 900 and 1100 cm^{-1} can be attributable to Si-O-Ca bonds (Meiszterics and Sinko, 2008). The bands in the 1600 to 2500 cm^{-1} range in the studied samples indicate the existence of unreacted calcium oxide. High-intensity bands of Ca silicate NPs and Ca silicate-PO$_4$ NPs can be observed at 1369 and 1415 cm^{-1}, respectively. These bands are caused by bending vibration modes in water molecules that are adsorbed dimerically and monomolecularly (Mansha et al., 2011) and are in the capillary condensation state.

Additionally, it should be noted that the Ca silicate-NO$_3$ NPs spectrum shows bands of lesser intensity when compared to the FTIR bands of untreated Ca silicate NPs (see Figure 2). Solonenko et al. (2018) found that Ca silicate-PO$_4$ NPs exhibit a sharp band at 1027 cm^{-1} due to stretching vibrations. The bands of calcium silicate NPs are different in all three spectra, suggesting the existence of several kinds of calcium silicates.

The XRD pattern of amorphous silica (Ca silicate), as shown in Figure 3, displays a distinctive hump at 2θ ~29.8°, indicating the formation of amorphous silica. The pattern of Ca silicate-NO$_3$ NPs reveals the crystalline phase. Notably, the smoothness of the

peaks indicates the removal of impurities in the pores of the Ca silicate NPs through numerous washings with deionized water. The pattern of Ca silicate-PO_4 NPs leads to numerous site exchanges, high selectivity, and capacity for different ions (Kotp, 2017).

The diameters of Ca silicate-NO_3 NPs and Ca silicate-PO_4 NPs were decreased from 88.5 nm to 87.9 nm and 62.3 nm during the treatment process, as illustrated in Figure 4. Due to this observation, the specific surface areas of powders and exchangeable processes have significantly increased (Sokolowska *et al.,* 2004).

Figure 5 shows SEM images depicting the surfaces of Ca silicate NPs, revealing noticeable gaps. These gaps may have developed during the first phase of potassium hydroxide's reaction with the surface of the silica. The quick shift of Ca silicate-PO_4 NPs suggests the swift contact of phosphoric acid with surfaces. According to Sharma *et al*. (2009), the phosphoric solution additives changed the surface, in addition to attacking ions on the surface, and dissolved them into the solution.

The preparation and reaction mechanisms of Ca silicate NPs involve dissolving them in an alkali solution and precipitating them in an acidic medium. Silica can be extracted from rice husks through this process. When using potassium hydroxide additives, silica is often extracted as potassium silicate. The chemical reaction is represented by the following formula (Equation 16):

$$SiO_2 + 2KOH = K_2SiO_3 + H_2O \tag{16}$$
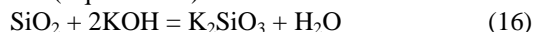
This fits well with Chun and Lee, 2020 theory (Equation 17).

$$CaSiO_3 + 2KCl = K_2SiO_3 + 2CaCl_2 \tag{17}$$

Using Ca silicate-NPs to remove $\mathbf{BO_3^{-3}}$, the surface of calcium atoms can pair up with nearby $\mathbf{BO_3^{-3}}$ to form ionic pairs (see Equation 18 and Figure 10). The silicate chains can offer several oxygen sites, facilitating interaction with nearby Na^+ by forming a stable Na-O ionic bond, aligning previous findings (Yang *et al*., 2019) (refer to Equation 19 and Figure 10).
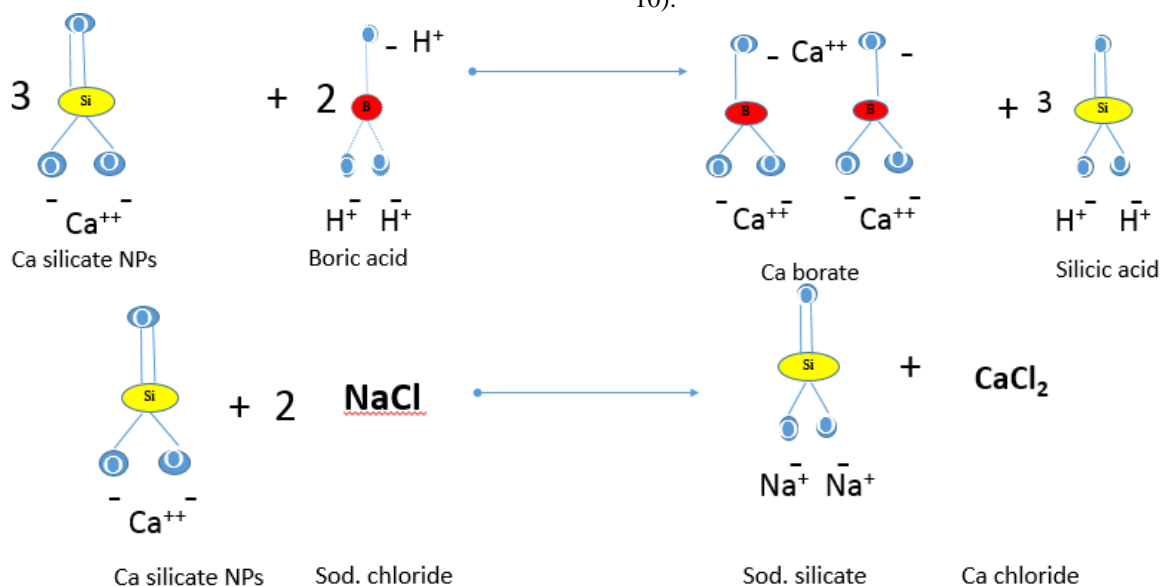

Fig. 10. The chemical structure of equations 18 and 19.

$$3Ca\,SiO_{3\,(Ca\,silicate-NPs)} + 2H_3BO_{3(boric\,acid)} \rightarrow (Ca)_3(BO_3)_{2(calcium\,borate)} + 3H_2SiO_{3\,(silicic\,acid)} \tag{18}$$

$$Ca\,SiO_{3\,(Ca\,silicate-NPs)} + 2Na\,Cl_{(sodium\,chloride)} \rightarrow Na_2SiO_{3(sodium\,silicate)} + CaCl_{2(calcium\,chloride)} \tag{19}$$
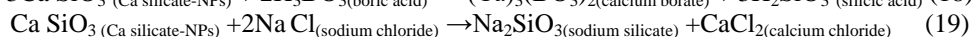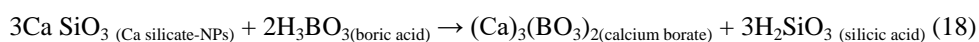
It was observed that the removal of BO_3^{-3} was higher than that of Na^+ when using the same adsorbent. According to the study conducted by Qiao *et al*. (2023), some Na^+ established fragile physical adsorption near the outer interphase, while others formed stable chemisorption with silicon chains by creating a Na-O-Si connection within the interphase zone of the calcium silicate surface.

Data in Tables 4 and 5 indicated that the correlation coefficients for the adsorption capacity were determined from the isotherm, Langmuir adsorption constant (K_L), and the constants K_F and n. It was demonstrated that the Langmuir model better fit the data than the Freundlich model (Jin *et al*., 2012).

The chemisorption between Na^+ and BO_3^{-3} and various adsorbents of Ca silicate NPs occurred according to pseudo-second-order kinetics. This preference was evident, as the pseudo-second-order kinetics model showed a better fit with R^2 than the pseudo-first-order kinetics model (Musie and Gonfa, 2022).

The potential surface charges of adsorbents may be altered by the presence of H^+ or OH^- ions in solutions. The rate of Na^+ removal increases when the

_____

pH of the salty solution is higher than 8, resulting in an increase in the negatively charged surface functional groups on adsorbents and electrostatic interactions between positively charged ions. This finding aligns with other studies (Cao *et al.*, 2016). Moreover, as the solution pH rises from 6.08 to 9.5, the removal percentage of BO_3^{-3} decreases from 18.98 to 7.70%, respectively. This decrease may be attributed to OH competition at the adsorption sites (see Fig. 6).

From the data presented in Table 6, the spontaneous nature of the adsorption process is demonstrated by the negative value of $\Delta G°$ obtained for the removal of Na^+ and BO_3^{-3}. The consistent decrease in the free energy value with the temperature rise suggests that the adsorption process is endothermic. The positive $\Delta G°$ values confirm the viability of the adsorption procedure and the specific removal of Na^+ and BO_3^{-3} by various adsorbents (Ca silicate NPs, Ca silicate-NO_3 NPs, and Ca silicate-PO_4 NPs). These findings suggest the potential of the adsorbents to remove Na^+ and BO_3^{-3} from salt-affected soil solutions, industrial wastewater, or other liquids that contain Na^+ and BO_3^{-3} at high concentrations.

The expected and experimental results for Ca silicate, Ca silicate-NO_3, and Ca silicate-PO_4 NPs and their ability to remove Na^+ and BO_3^{-3}, as well as their R^2 and R^2_{adj} values, are tabulated in Table 7. In the 31 trials collected from the studied area, the parameters (pH, concentrations, contact time, and temperature) were optimized using a multivariate design. These variables, or components, were chosen for the study because they substantially impact the adsorption process.

According to Miller and Miller (2005), the large *F* ratio implies that the regression equations (Table 9) can effectively characterize the variability in response. The accompanying *p*-value determines whether the *F* ratio is significant enough to imply any significant effect.

Table 7 establishes the mathematical correlations connecting the observed response (removal percent %) of Na^+ or BO_3^{-3} and the model variables. These connections are defined by the regression equations (10-15) produced by the Minitab statistical software. These results demonstrate that the effects of large *F* ratios with their corresponding *p*-values less than 0.05 were found with the pH and concentration factors.

In Figures 7 (a and b), the plots of residuals versus predictions exhibited a random distribution pattern, confirming the appropriateness of the regression model (Hasan *et al.*, 2009).

Figures 8 and 9 show the interactive effects of parameters (pH, concentrations, contact time, and temperature) on the removal percentage of Na^+ and BO_3^{-3} by Ca silicate-PO_4 NPs. Figures 8 and 9 displayed the surface plots of the expected response of the removal percentage of Na^+ and BO_3^{-3} by Ca silicate-PO_4 NPs against two of the four studied

parameters (pH, concentrations, contact time, and temperature); the other two parameters were set to be at the medium values. According to Yasin *et al.* (2013), the diagram surface's height value determines the expected removal percentage response.

Table 10, produced from the Minitab statistical software, displayed the anticipated optimum conditions (pH, concentrations, contact time, and temperature) for the removal percentage of Na^+ cation and BO_3^{-3}. Under these conditions, the maximum removal percentages (%) by the various adsorbents of Ca silicate NPs reached their highest values.

Table 11 indicates significant effects in soil pH and EC, and several elements such as Na, Ca, B, Si, Al, Fe, Sr, and Mn in dill plants occurred at additional rates.

Although the total boron concentration in the studied soil was 99.0 ppm, the boron uptake by dill plants was below the critical level. This may be because calcium silicate NPs have a strong affinity for boron. Changes in boron concentration in the soil solution can significantly impact the quantity of boron absorbed by dill plants (Brdar-Jokanović, 2020).

There was a significant relationship between Ca silicate NPs and Na^+ contents in dill plants. Adding Ca silicate NPs lowered the contents of Na^+ in the leaves of dill plants. This behavior aligns with the hypothesis conducted by Gong *et al.* (2006), suggesting that adding Si complexes reduced the translocation of Na^+ from roots to shoots. This finding agrees with the study of Ahmad *et al.* (1992), who found that adding silicate reduced the Na^+ contents in rice plant leaf blades. According to Elsakhawy *et al.* (2018), silicon is also known to reduce the absorption of Na^+ by increasing the $K^+:Na^+$ absorption and reducing the toxicity of other elements.

Table 12 shows the comparison of removal of Na^+ and BO_3^{-3} by some different adsorbents in the present study, including studies by Hilal *et al.* (2011), Ferreira *et al.* (2005), Ay *et al.* (2007), You *et al.* (2001), Soliman *et al.* (2019), Musie and Gonfa (2022), Shokrian *et al.* (2015), Sommerfeldt (1961), Agudelo *et al.* (2016), Hou *et al.* (2017), and Chaari *et al.* (2020). The percentage obtained from these studies is considered a reliable indicator of removing Na^+ and BO_3^{-3} from the salt-affected soils. These removal percentages (%) were improved when Ca silicate NPs were treated with 0.1M HNO_3 and 0.1M H_3PO_4.

5. Conclusions

In this work, various Ca silicate NPs were examined as adsorbents to remove Na^+ and **BO_3^{-3}** from solutions and soil. The structure of the adsorbents was characterized using SEM, XRD, FTIR, and DLS. The studied parameters were pH, concentrations, contact time, and temperature, with the highest removal percentage (%) achieved by Ca silicate-PO_4 NPs (36.85% for Na^+ and 46.42% for **BO_3^{-3}**). The

_____

Langmuir isotherm model could provide a suitable interpretation of the adsorption data and the pseudo-second-order used to characterize the adsorption process. The uptake of Na^+ and boron by dill plants was reduced when various adsorbents of Ca silicate NPs were added, whereas the uptakes of both Ca and Si were increased. Finally, we may conclude that manufacturing Ca silicate NPs from leftover agricultural materials is a successful approach for enhancing the ability of dill plants to grow in saline soils and can increase the disposal of agro-industrial wastes such as rice husks.

6. Conflicts of interest

There are no conflicts to declare.

7. Formatting of funding sources

There is no funding agency.

References

Abd-Elzaher MA, El-Desoky MA, Khalil FA, Eissa MA, Amin AEA (2022). Interactive Effects of K-Humate, Proline and Si and Zn Nanoparticles in Improving Salt Tolerance of Wheat in Arid Degraded Soils. Egypt. Egyptian Journal of Soil Science, 62(3): 237-251.

Abdrabou MR, Gomah HH, Darweesh AM, Eissa MA, Selmy SAH (2022). Response of Saline Irrigated Quinoa (Chenopodium quinoa Wild) Grown on Coarse Texture Soils to Organic Manure. Egyptian Journal of Soil Science, 62(2): 169-178.

Agudelo N, Hinestroza JP, Husser J (2016). Removal of sodium and chloride ions from aqueous solutions using fique fibers (Furcraea spp.). Water Science & Technology, 73(5), 1197-1201.

Ahmad R, Zaheer SH, Ismail S (1992). Role of silicon in salt tolerance of wheat (Triticum aestivumL.). Plant Science 85, 43–50.

Awad EA, Mohamed IR, Abd El-Hameedb AM, Zaghloul EA (2022). The Co-addition of soil organic amendments and natural bio-stimulants improves the production and defenses of the wheat plant grown under the dual stress of salinity and alkalinity. Egyptian Journal of Soil Science, 62(2): 137-153.

Ay AN, Zümreoglu-Karan B, Temel A (2007). Boron removal by hydrotalcite-like, carbonate-free Mg–Al–NO3-LDH and a rationale on the mechanism. Microporous and Mesoporous Materials 98(1–3), 1–5.

Bonilla I, González-Fontes A (2011). Salt Stress in Vascular Plants and Its Interaction with Boron Toxicity, Plants and Environment, Hemanth KN. Vasanthaiah and Devaiah Kambiranda (Ed.), ISBN: 978-953- 307-779-6, 227-240 p.

Brdar-Jokanović M (2020). Boron Toxicity and Deficiency in Agricultural Plants. International Journal of Molecular Sciences 21(4), 1424.

Cao D, Jin X, Gan L, Wang T, Chen Z (2016). Removal of phosphate using iron oxide nanoparticles synthesized by eucalyptus leaf extract in the presence of CTAB surfactant. Chemosphere 159, 23–31.

Chaari I, Medhioubb M, Jamoussi F, Hamzaoui AH (2020). Acid-treated clay materials (Southwestern Tunisia) for removing sodium leuco-vat dye: Characterization, adsorption study and activation mechanism. Journal of Molecular Structure 1223, 128944.

Chun J, Lee JH (2020). Recent Progress on the Development of Engineered Silica Particles Derived from Rice Husk. Sustainability 12, 10683.

Debona D, Rodrigues FA, Datnoff LE (2017). Silicon's role in abiotic and biotic plant stresses. Annual Review of Phytopathology 55, 85–107.

Delfine S, Loreto F, Pinell P, Tognetti R, Alvino A (2005). Isoprenoids content and photosynthetic limitations in rosemary and spearmint plants under water stress. Agric. Eco-systems Environ. 106, 243-252.

Elsakhawy T, Omara AE, Alshaal T, El-Ramady H (2018). Nanomaterials and Plant Abiotic Stress in Agroecosystems. Environment, Biodiversity & Soil Security 2(2018), 73 – 94.

El-Sayed SF, Hassan HA, Ali AM, Gibrael AA (2022). Effect of foliar-applied potassium silicate on growth, yield, fruit quality and antioxidant activity of tomato plants grown under deficit irrigation. International Journal of Health Sciences 6(S6), 10012–10032.

El-Sherpiny MA, El-Bakry FA, Ibrahim NR, El-Shaboury HA (2023). Role of compost, biochar and sugar alcohols in raising the maize tolerance to water deficit conditions. Egyptian Journal of Soil Science, 63(1): 67-81.

FAO (2003). Chapter 2: Food security: Concepts and measurement. In FAO (Ed.), Trade reforms and food security (pp. 25-34). Rome. Food and Agriculture Organization of the United Nations.

Ferreira OP, Moraes SG, Duran N, Alves OL (2005). High efficiency removal of boron from water by hydrotalcite-like compounds. In: REWAS'04-Global symposium on recycling. Waste Treatment and Clean Technology, 2867–2868.

Gavlak R, Horneck D, Miller RO, and Kotuby-Amacher J. (2005). Soil, plant and water reference methods for the western region. WREP-125, 3rd Edition, Fort Collins, CO.

Gong HJ, Randall DP, Flowers TJ (2006). Silicon deposition in the root reduces sodium uptake in rice (Oryza sativaL.) seedlings by reducing bypass flow. Plant, Cell and Environment 29, 1970 – 1979.

Grattan SR, Díaz FJ, Pedrero F, Vivaldi GA (2015). Assessing the suitability of saline wastewaters for irrigation of Citrus spp.: Emphasis on boron and specific-ion interactions, Agricultural Water Management 157, 48-58.

Hasan S, Srivastava P, Talat M (2009). Biosorption of Pb(II) from water using biomass of Aeromonas hydrophila: central composite design for optimization of process variables. Journal of Hazardous Materials 168(2-3), 1155–1162.

Hilal N, Kim GJ, Somerfield C (2011). Boron removal from saline water: A comprehensive review. Desalination 273, 23–35.

Hou D, Li D, Yu J, Zhang P (2017). Insights on capillary adsorption of aqueous sodium chloride solution in the nanometer calcium silicate channel: A molecular dynamics study. The Journal of Physical Chemistry C 121(25), 13786-13797.

Jackson ML (1973). Soil Chemical Analysis. Prentice Hall of India Pvt. Ltd., New Delhi, 498.

Jalhoum MEM, Mazrou YSA, Hassan MA, Farag FM, Abdellatif MA, Abdelsamie EA, Amin MA, El Baroudy AA, Belal AA, Shokr MS (2022). Modeling of Agro-Ecological Zones for Sustainable Agriculture

Development in Halayeb Area, Egypt. Egyptian Journal of Soil Science, 62(1): 55-71.

Jin YJ, Liu F, Tong MP, Hou YL (2012). Removal of arsenate by cetyltrimethylammomium bromide modified magnetic nanoparticles. Journal of hazardous materials 227, 461-468.

Kotp YH (2017). Controlled synthesis and sorption properties of magnesium silicate nanoflower prepared by a surfactant-mediated method. Separation Science and Technology 52(4), 657-670.

Kumar R (2012). Human Resource Information System: An Innovative Strategy or Human Resource Management. Gian Jyoti E-Journal 1, 1-12.

Meiszterics A, Sinko K (2008). Sol-Gel Derived Calcium Silicate Ceramics. Colloids and Surfaces A 319(1-3), 143-148.

Miller JN, Miller JC (2005). Statistics and chemometrics for analytical chemistry. Pearson/Prentice Hall, London.

Minitab Statistical Software (2023). LLC., Quality Plaza, 1829 Pine Hall Rd, State College, PA, 16801-3210, United States.

Musie W, Gonfa G (2022). Adsorption of sodium from saline water with natural and acid activated Ethiopian bentonite. Results in Engineering 14, 100440.

Nicholson G (1984). Methods of Soil, Plant and Water Analysis. N.Z. Forest Service. F. R. I. Bulletin, 70.

Pavia DL, Lampman GM, Kriz GS, Vyvyan JR (2009). Infrared Spectroscopy. In: Introduction to Spectroscopy, Cengage Learning, Washington DC, 15-30.

Qiao G, Hou D, Li W, Yin B, Zhang Y, Wang P (2023). Molecular insights into migration of heavy metal ion in calcium silicate hydrate (CSH) surface and intra-CSH (Ca/Si= 1.3). Construction and Building Materials 365(15), 130097.

Richard LA (1954). Diagnosis and improvement of saline and alkali soils. USDA Handbook 60. Washington DC. 160 pp.

Sharma K, Dixit A, Singh S, Jagannath, Bhattacharya S, Prajapat CL, Sharma PK, Yusuf SM, Tyagi AK, Kothiyal GP (2009). Preparation and studies on surface modifications of calcium-silico-phosphate ferrimagnetic glass-ceramics in simulated body fluid. Materials Science and Engineering: C 29(7), 2226-2233.

Shelke VR, Bhagade SS, Mandavgane SA (2010). Mesoporous Silica from Rice Husk Ash, Bulletin of Chemical Reaction Engineering & Catalysis 5 (2), 63 – 67.

Shokrian F, Solaimani K, Nematzadeh GH, Biparva P (2015). Removal of NaCl from aqueous solutions by using clinoptilolite. International Journal of Farming and Allied Sciences 4(1), 50-54.

Simon JE, Chadwick AF, Craker LE (1984). Herbs: An Indexed Bibliography, 1971-1980, the scientific literature on selected herbs and aromatic and medicinal plants of the temperate zone, p: 770. Archon Books, Hamden, CT, the Shoe String Press, Inc., USA.

Singh D, Seager R, Cook BI, Cane M, Ting M, Cook E, Davis M (2018). Climate and the global famine of 1876-78. Journal of Climate 31(23), 9445- 9467.

Sokolowska Z, Hajnos M, Elias EA, Alaily F (2004). Characteristics of the specific surface area of Vertisols from the Gezira region in Sudan. International agrophysics 18, 83-90.

Soliman ER, Kotp YH, Souaya ER, Guindy KA, Ibrahim RGM (2019). Development the sorption behavior of nanocomposite Mg/Al LDH by chelating with different monomers. Composites Part B: Engineering 175, 107131.

Solonenko AP, Blesman AI, Polonyankin DA, Gorbunov VA (2018). Synthesis of Calcium Phosphate and Calcium Silicate Composites. Russian Journal of Inorganic Chemistry 63(8), 993–1000.

Sommerfeldt GT (1961). Effects of Anions on the Sodium Adsorption Capacity and Electrophoretic Mobility of Sodium Saturated Utah Bentonite. All Graduate Theses and Dissertations, Spring 1920 to Summer 2023. 3601.

Sukhdev SH, DevDutt R, Karan V (2006). Compendium of Medicinal and Aromatic Plants ASIA. ICS-UNIDO, AREA Science Park   Padriciano 99, 34012 Trieste, Italy.

Swelam A, Farag A, Ramasamy S, Ghandour A (2022). Effect of Climate Variability on Water Footprint of Some Grain Crops under Different Agro-Climatic Regions of Egypt. Atmosphere, 13(8): 1180.

Todkar BS, Deorukhkar OA, Deshmukh SM (2016). Extraction of Silica from Rice Husk. International Journal of Engineering Research and Development 12(3), 69-74.

USDA (2014). Kellogg Soil Survey Laboratory Methods Manual, Soil Survey Investigations Report No. 42 Version 5.0.

Yang J, Jia Y, Hou D, Wang P, Jin Z, Shang H, Zhao T (2019). Na and Cl immobilization by size controlled calcium silicate   hydrate nanometer pores. Construction and Building Materials 202, 622–635.

Yasin Y, Mohamad M, Ahmad FB (2013). The application of response surface methodology for lead ion removal from aqueous solution using intercalated tartrate-Mg-Al layered double hydroxides. International Journal of Chemical Engineering 2013, 937675.

You Y, Vance GF, Zhao H (2001). Selenium adsorption on Mg–Al and Zn–Al layered double hydroxides. Applied Clay Science 20(1–2):13–25.

Zaman M, Shahid SA, Heng L, Shahid SA, Zaman M, Heng L (2018). Soil salinity: Historical perspectives and a world overview of the problem. Guideline for salinity assessment, mitigation and adaptation using nuclear and related techniques, 43-53.